JOURNAL OF MATERIALS SCIENCE 25 (1990) 3072–3078

Defect microstructure and dehydroxylation mechanism of interstratified phyllosilicates: a TEM study

P. SHEN*, S. L. HWANG*, H. T. CHU‡
*Institute of Materials Science and Engineering, National Sun Yat-Sen University, Kaohsiung, Taiwan
‡Central Geological Survey, PO Box 968, Taipei, Taiwan

The dehydroxylation mechanism of natural phyllosilicates containing interleaved chlorite and serpentine layers and defects such as dislocation, stacking faults, microcleavage and folding were studied by transmission electron microscopy. Upon irradiation of electrons, epitaxial magnesium hydroxide was formed after phyllosilicates and the microcracks were preferentially formed at interleaved areas, stacking faults and other defects. Microcracks then extended along basal layers and coalesced to form larger cracks. Prolonged exposure to electron radiation resulted in the complete dehydration of phyllosilicates into periclase particles of several nanometres in size and probably other microcrystallites within the residual silica matrix.

1. Introduction

Thermal decomposition of carbonates, hydroxides and hydrosilicates generally known as calcination is commonly used to produce sinterable powder in the ceramics industry. Generally speaking, decomposition of these materials involves removal of hydroxyl radicals from the layered structures and is closely related to the partial pressure of H_2O or CO_2. Kinetic studies on the removal of the hydroxyl radicals by measuring weight loss as a function of time and temperature have been conducted in air or under vacuum conditions for carbonate [1], brucite [2–8], kaolinite and halloysite [9–11].

The structural changes which occur during H_2O or CO_2 loss have been studied by various authors. By electron radiation on basal layers (top view) using transmission electron microscopy (TEM) technique, Goodman [12] concluded that the decomposition of brucite occurs in two stages: first, there is a small shrinkage in the basal plane, and the resulting strain causes a collapse of the plane down the original (0 0 0 1) of magnesium hydroxide. However, the electron diffraction measurements of the lattice parameter of brucite decomposed *in situ* either by electron beam heating or hot stage heating [13] is not consistent with Goodman's hypothesis of homogeneous nucleation [12]. Since 1958 great progress on TEM imaging has been made, therefore, more detailed information about the structural changes at various orientations during decomposition of layered minerals could be obtained by studying their lattice images. It is known that the heat produced by electron bombardment causes the disappearance of (0 0 2) fringes of chlorite [14], and the formation of voids in kaolinite [15]. It also causes loss of crystallinity in kaolinite [15] and chrysotile [16].

The interlayering in phyllosilicates, particularly among clay minerals has been well documented ([17–25] and literature cited herein) e.g. ordered and disordered chlorite–biotite interstratification as alteration products of chlorite was observed [24]; the interstratification of chlorite with serpentine or mica was observed in pelitic rocks of low grade metamorphism ([25] and literature cited herein) and the possible ambiguous TEM interpretation of mixed layers discussed [25]. The stacking disorder in chlorite has been studied by high resolution transmission electron microscopy (HRTEM) [26, 27]. Deformation defects such as microcleavage, bending and kinking have also been found in phyllosilicates by HRTEM ([27] and literature cited herein). The coherent exsolution phases termed GP (Guinier–Preston) zones as in alloys have also been observed in phyllosilicates [18]. The GP zones, interlayers, and deformed defects may cause considerable strain in the surrounding structure, and are likely to be the preferred sites for dehydroxylation. The disturbance, if any, of the stacking fault during electron irradiation may also play an important role in the decomposition of the basal layers of phyllosilicates. Data from a survey of TEM observations of micas and other phyllosilicates which show fissures imply that the fissures are directly associated with the diffusivity of the interlayer cations [28].

In the present study, the one-dimensional lattice images of the interstratified phyllosilicates of local occurrence were investigated by TEM with a view to looking for the causes of the undulatory extinction observed under polarized microscopy [29] and to studying the dehydroxylation process by electron beam heating. The edge-on view of the layered structures and the defect microstructure observed during electron irradiation provide information about the decomposition mechanism.

0022–2461/90 $03.00 + .12

2. Experimental details

Naturally occurring hand specimens of podiform chromitite containing dominantly chromium spinel, phyllosilicates, carbonates, and oxides were recovered from Kenting melange, southern Taiwan [29]. According to the electron probe microanalysis (EPMA), the phyllosilicates surrounding the brecciated chromium spinel grains consist of chlorite (clinochlore) and serpentine whose chemical formulae are [29] $(Ca_{0.01}Cr_{0.02}Al_{1.09}Fe_{0.09}Mg_{4.78})[(Si_{2.91}Al_{1.09})O_{10}](OH)_8$ and $(Ca_{0.01}Fe_{0.08}Cr_{0.01}Al_{0.05}Mg_{2.85})[(Si_{1.94}Al_{0.06})O_5](OH)_4$, respectively.

The phyllosilicates selected from thin sections were ion-milled to electron transparency for TEM (using a JEOL 200CX instrument) studies. Ion milling involves heating the sample in vacuum, however the decomposition of phyllosilicates is minor if the accelerating voltage and current were reduced. Electron irradiation at 200 kV, under 10^{-6} atm, were adopted as the heating source for dehydroxylation of the phyllosilicates. The edge-on view of the lattice images subjected to various electron doses was taken with reflections passing through a 40 μm objective aperture centred on the incident beam. Most of the lattice images were selected from experimental through-focus series generally recorded in the 80 to 120 nm range of underfocusing. Conventional bright-field images (BFI), dark-field images (DFI) and the corresponding selected area diffraction (SAD) patterns were also taken during observation. Energy dispersive X-ray (EDX) analysis coupled with scanning transmission electron microscopy (STEM, using also JEOL 200CX instrument at 40 kV) was used for the qualitative chemical analysis on TEM sample foils.

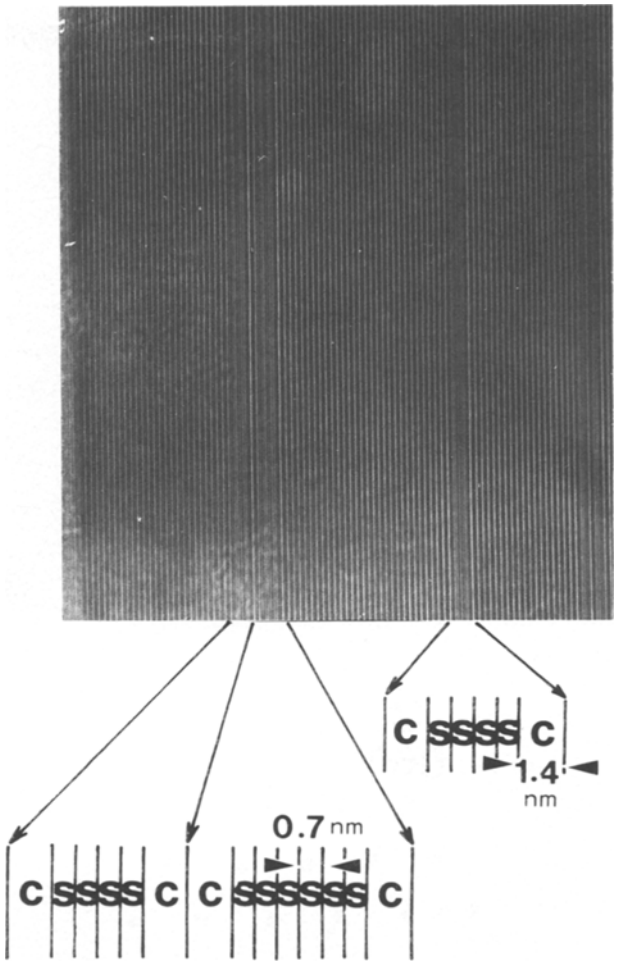

Figure 1 Transmission electron micrograph of chlorite-rich area of phyllosilicates showing intergrowths of individual serpentine (S) and chlorite (C) basal layers in chlorite matrix.

3. Results

3.1. Before dehydroxylation

Phyllosilicates in chromitite can generally be divided into the chlorite-rich and the serpentine-rich layers which may be up to several micrometres in thickness according to their optical properties, SAD patterns and the EPMA analysis [29]. In the transition zone between chlorite and serpentine, the interstratified 1.4 and 0.7 nm basal layers along with their multiples were characteristic. However, the multiples, e.g. 2.1 nm, are generally not enough to give the diffracted spots in the SAD pattern. Such a capability to give various stacking sequences has already been pointed out and interpreted as a likely polytypic behaviour of the 0.7 nm phase [23, 25] although an ambiguity due to imaging conditions may arise in the TEM image interpretation of a (2×0.7) nm possible repeated stacking sequence, and a 1.4 nm chlorite structure, particularly when they are mixed [25]. Significant packets of 0.7 nm layers may be sandwiched between blocks of 1.4 nm layers. Also individual 0.7 nm layers, generally randomly mixed with chlorite layers (indexed according to SAD patterns) were also found (Fig. 1). Structures similar to such 0.7 nm layers within 1.4 nm layers were also observed ([25] and literature cited herein) and the 0.7 nm phase interpreted as the precursor of 1.4 nm chlorite [25] according to the chlorite-synthesis study [30].

The semi-random [26, 31] or complete-random [27] stacking sequence of the chlorite layers cannot be resolved in one-dimensional lattice image. However, by tilting away from the edge-on orientation, stacking faults were revealed by DFI (Fig. 2a). These stacking faults have fringes bound by dislocations and occasionally form loops (Fig. 2a). The corresponding top view (Fig. 2b) shows the modulated contrast due to the combined effects of Moire and dislocation contrast. Exact determination of the chlorite polytypes, especially the shift vectors across the talc-like and brucite-like sheets, is beyond the scope of the present TEM study, because complete specification of chlorite polytypism requires either HRTEM combined with X-ray diffraction analysis or HRTEM images from more than one major zone of the same crystal [26]. However, the Moire fringes running in three directions (Fig. 2b) and the corresponding SAD pattern (Fig. 2c) indicate that three basic stacking variants probably dominate in the chlorite phase. Local bending (Fig. 3a) or mismatching (Fig. 3b) of the basal layers of chlorite results in the offset of diffraction streaks in the SAD pattern. Diffraction streaks along c^* are likely to be due to stacking variants and stacking faults of the basal layers. The deformation defects such as microcleavage (Fig. 3c) and folding or kinking (Fig. 3d) are also present in chlorite.

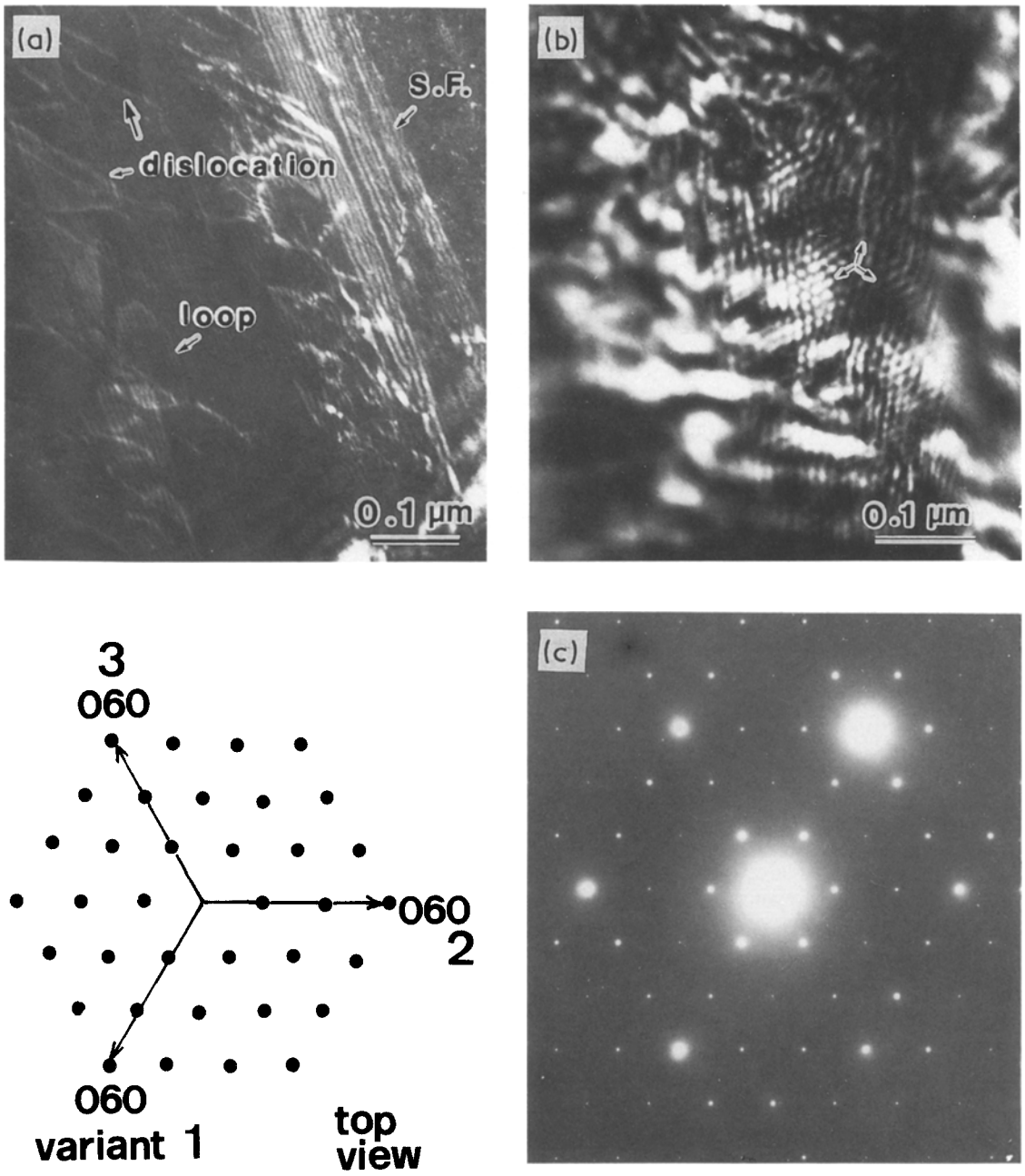

Figure 2 Transmission electron micrograph showing (a) DFI of stacking faults, dislocations and loops after tilting from edge-on orientation of chlorite, (b) top view of the same area showing Moire fringes and dislocation which gives modulated contrast, (c) SAD pattern with electron beam perpendicular to the stacking faults of chlorite basal layers.

3.2. Decomposition observations

During TEM observations, the dislocations in the interstratified chlorite and serpentine move, and modify the stacking sequence of the phyllosilicates. In addition to this process, the disappearance or appearance of the (0 0 2) fringes of chlorite under the electron beam likely to be due to a "defocalisation" or thickness effect [25] was observed and epitaxial magnesium hydroxide having the following preferred crystallographic relationship to the phyllosilicates

$$(0\,0\,1)\text{phyllo}//(0\,0\,0\,1)\text{Mg(OH)}_2;$$

$$(0\,6\,0)\text{phyllo}//(1\,1\,\bar{2}\,0)\text{Mg(OH)}_2$$

was found (Fig. 4). The diffraction spots of Fig. 4 correspond to partially decomposed phyllosilicates and brucite, whereas the rings in Fig. 4 can be indexed as oxides having rock salt structure and are diffracted from particles less than 10 nm in size as shown in the DFI (Fig. 5). Note that the preferred orientation of MgO particles occurs as shown by the {2 2 0} arc superimposed on the {2 2 0} ring in Fig. 4. These preferentially oriented MgO particles have their (1 1 1) planes normal to the electron beam direction in Fig. 4. Since {2 0 0} diffraction spots of the preferentially oriented MgO particles are not at Bragg condition in Fig. 4, no arc was found on the (2 0 0) ring. By comparing the arcs of MgO and adjacent diffraction spots of brucite the following crystallographic relationships are obtained

$$(0\,0\,0\,1)\text{Mg(OH)}_2//(1\,1\,1)\text{MgO};$$

$$[1\,1\,\bar{2}\,0]\text{Mg(OH)}_2//[1\,0\,\bar{1}]\text{MgO}$$

which are consistent with those reported previously [1, 4, 7, 12, 13]. Since magnesium is the most abundant cation in the undecomposed chlorite and serpentine, the newly formed oxide particles are most likely to be

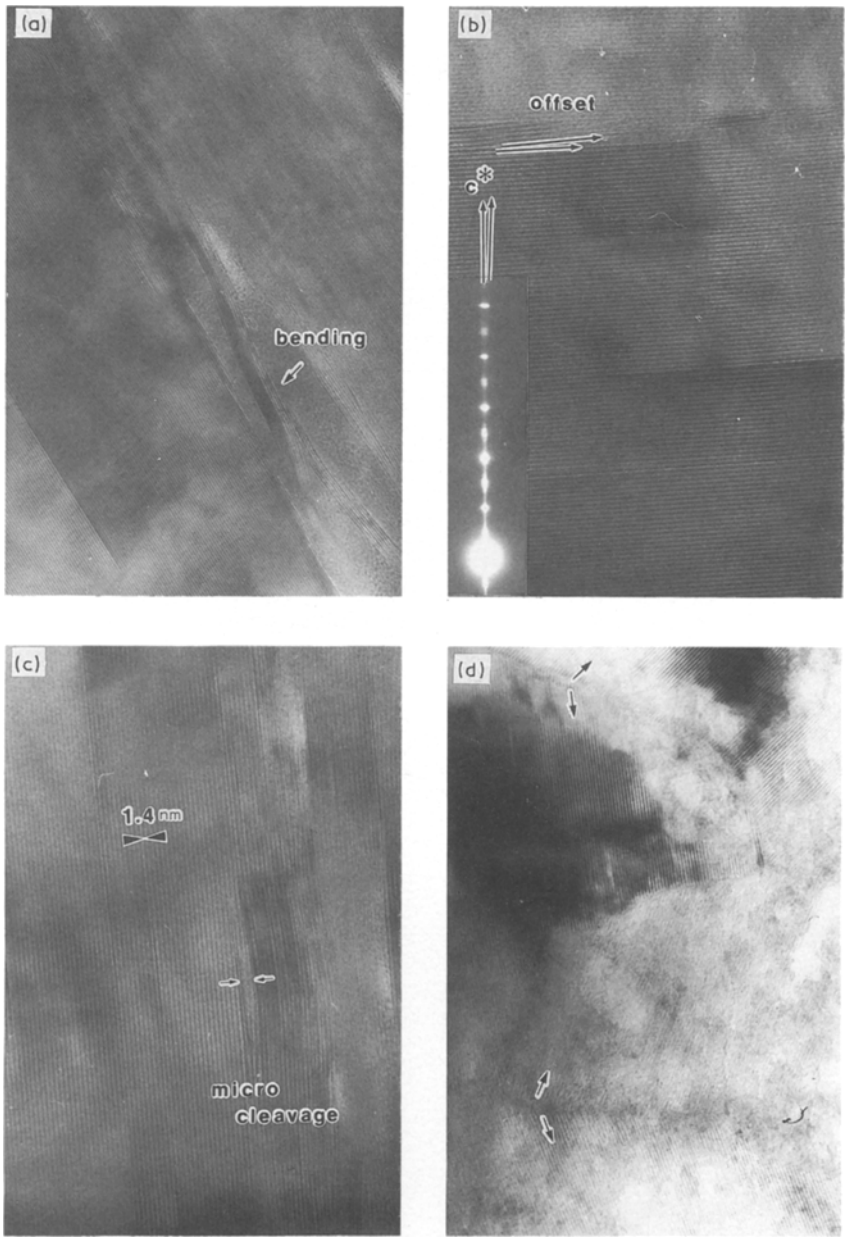

Figure 3 Transmission electron micrograph of chlorite showing (a) bending, (b) mismatching, (c) microcleavage and (d) folding of the basal layers viewed edge-on.

periclase, MgO containing a small amount of alloying elements though not enough to analyse by the STEM–EDX technique. With still longer exposure to electron irradiation, the amount $Mg(OH)_2$ decreases whereas MgO increases. The residuals of the decomposed phyllosilicates probably also contain amorphous silica as indicated by the diffuse intensity in the SAD pattern and the detection of silicon in the EDX analysis. However the presence of a small quantity of microcrystallites such as quartz [19] or other oxides in the decomposed product of phyllosilicate cannot be excluded because cations other than Si^{+4} are present in the parent phyllosilicates.

3.3. Formation of cracks

After a few minutes exposure to the electron beam, a large number of microcracks having widths of the individual layers and length measured tens of nanometres are formed at stacking faults, interleaved areas and deformation defects, and gives strain contrast (Fig. 6) in the interstratified phyllosilicates. These microcracks are similar to the lenticular fissures observed in other phyllosilicates ([28] and literature cited therein). The microcracks then extend in length by coalescence of the individual ones parallel to the basal layers until large cracking and separation occurs. Extensive fissuring (or cracking) network of decomposed product was also observed (Fig. 7).

4. Discussion

4.1. Defect microstructure

According to the chemical formula the present chlorite, with its high content of magnesium and low content of aluminium and iron can be classified as clinochlore. It follows that most of the octahedral layers in chlorite remain tri-octahedral and the transition from chlorite to serpentine layers may not be a sharp boundary as indicated by optical microscopy observations. The 0.7 nm layer of serpentine could probably be the precursor of the 1.4 nm chlorite layer as previously

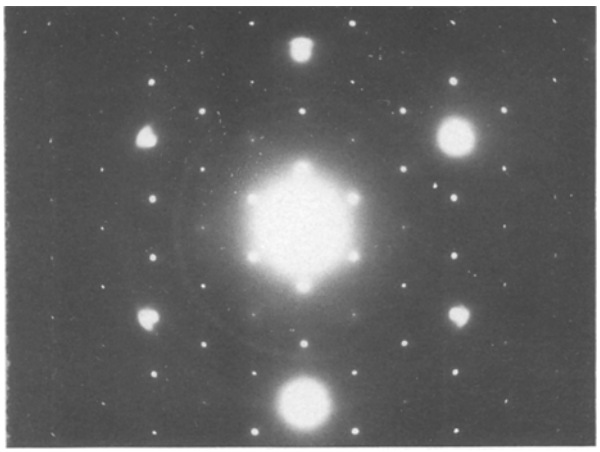

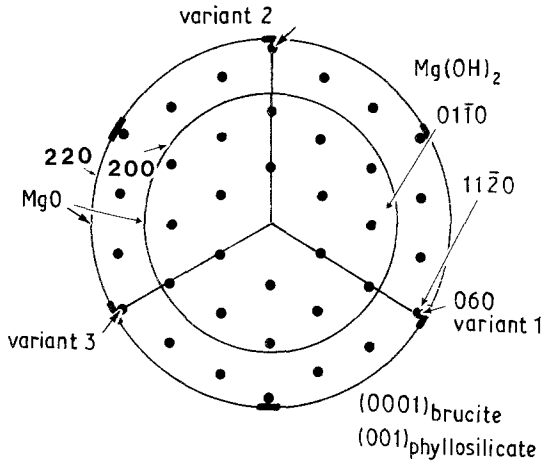

Figure 4 SAD pattern and schematic indexing of interstratified chlorite–serpentine taken after a few minutes of electron irradiation, showing epitaxial magnesium hydroxide and polycrystalline magnesium oxide formed by decomposition of the phyllosilicates.

suggested [25, 30]. The undulatory extinction of both chlorite and serpentine observed by polarized microscopy [29] is closely related to the strain contrast which is in turn caused by the combined effects of composition variation, stacking faults, deformation defects, and the distortion of the ideal octahedral and/or tetrahedral networks as revealed by the present defect microstructure observations. The deformation defects in chlorite were probably formed by plastic deformation during ocean floor metamorphism subsequent to the plastic deformation episodes of the host chromium spinel grains [32].

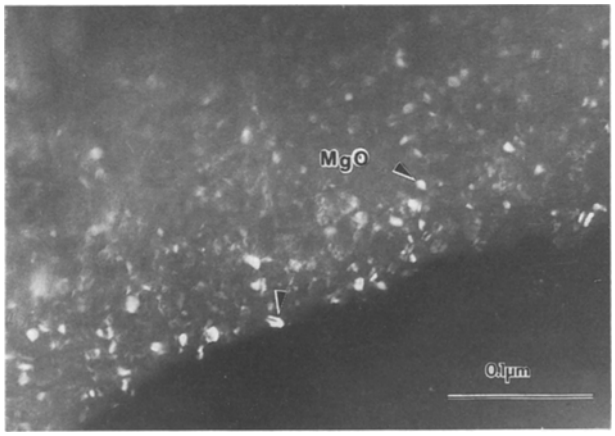

Figure 5 Transmission electron micrograph (DFI) of decomposed phyllosilicates showing magnesium oxide particles (bright) in residual silica matrix.

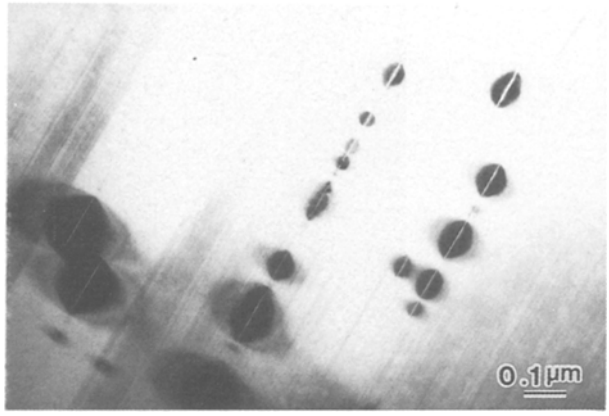

Figure 6 Transmission electron micrograph of interstratified chlorite–serpentine showing coalesced microcracks parallel to the basal layers.

4.2. Factors of dehydroxylation

Electron bombardment and heating effects are the main factors causing damage of the sample foil during TEM observations. The heating effect is responsible for homogeneous nucleation and growth of the periclase particles and formation of the residual silica during dehydroxylation of the phyllosilicates. The additional effects of vacuum and electron bombardment can significantly lower the dehydroxylation temperature and accelerate formation of the cracks.

4.3. Dehydroxylation mechanism

The coherent brucite–serpentine intergrowths have been reported in the high resolution TEM study of carbonaceous chondrite [33]. The epitaxial brucite diffraction spots do not appear initially until after several minutes of electron irradiation of the present phyllosilicates sample, indicating that brucite was formed by dehydroxylation rather than being inherent

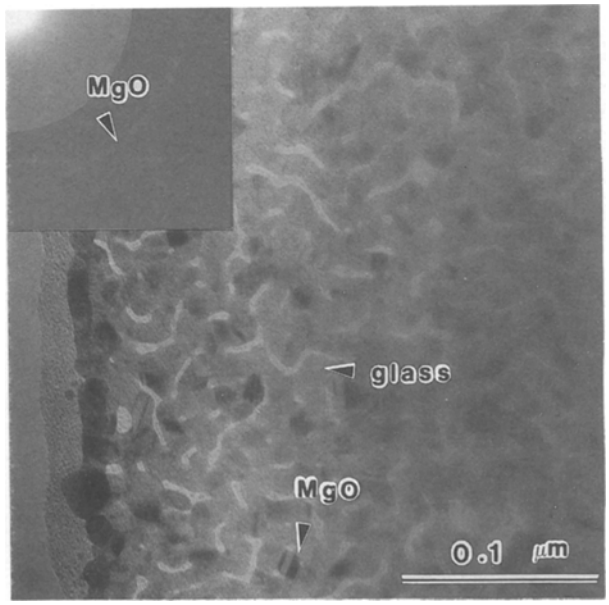

Figure 7 Transmission electron micrograph of MgO showing crack network formed during the decomposition of brucite.

in the hand specimens. In contrast to the selective decomposition of brucite sheets in heated chlorite by X-ray diffraction study [34], electron irradiation of clinochlore chlorite causes preferential damage of talc-like layers rather than brucite-like layers [26]. The chlorite–brucite transformation is probably facilitated by movement of the stacking faults and dislocations during electron irradiation so that the brucite-like sheets can be detached. It is also likely that cation-diffusion-induced formation of fissures play a role in the chlorite–brucite transformation analogous to the transformation of paragonite into pyrophyllite [28].

The subsequent decomposition of brucite into periclase could initially retain the preferred orientation relationship as indicated by arcs of MgO adjacent to the diffraction spots of partially decomposed brucite. This stage is not obvious in the present observation due to interference of the diffraction spots of the residual phyllosilicates and the subsequent loss of the preferred orientation of MgO particles. The loss of preferred orientation relationship suggests a likely nucleation and growth mechanism of MgO particles beyond a critical size similar to the oxidation in other composition systems ([35] and literature cited therein) although a complete film of the phenomenon as a function of time was not obtained due to the fast decomposition of brucite and growth of MgO particles. The preferred orientation relationships among phyllosilicates, brucite and periclase are due to the correlation between oxygen octahedra in the parent and product solids as suggested for the decomposition of brucite and magnesite [13].

4.4. Mechanism of crack formation

The present TEM study indicates that cracks or pores form preferentially at stacking faults, interleaved layers or at the deformation defects such as microcleavage and mismatched area, indicating the dehydroxylation of interstratified chlorite–serpentine is an inhomogeneous process, as has been suggested for the dehydroxylation of kaolinite, halloysite dickite and talc [15]. The stress that arises in conjunction with the movement of dislocation probably also plays a role in the nucleation of microcracks. It has been reported [36] that the diagonal intergrowths of brucite within amphibole layers are the preferred sites for the formation of pores and the adsorption of gases. The large cracks parallel to the stacking layers of the present phyllosilicates are probably due in part to the decomposition of interstratified serpentine layers if any, forming brucite and therefore pores although the loss of the 0.7 nm fringes could also be due to thickness or defocalization effects [25]. It is also likely that the fissures are directly associated with the diffusivity of interlayer cations in phyllosilicates as previously suggested [28]. The occurrence of the lenticular fissures in paragonite has been attributed to the loss of sodium which causes collapse of the paragonite structure to a pyrophyllite-like structure [28]. According to [28], release of the resulting elastic strain associated with the local collapse may cause mechanical separation of paragonite layers along (0 0 1) and the propagation of the fissures are likely to occur along the interlayers having weaker bonding than that across tetrahedral and octahedral layers.

The irregular pores in local areas are probably formed after the local disturbances by the combined affects of thermal expansion, capillary and dehydroxylation. According to Kim *et al.* [13], the small MgO particles which have high excess surface energy [37] and are in contact may aggregate spontaneously at a certain scale to reduce the excess energy. At the same time a stress will develop along the reaction interface to create network-like cracks in brucite.

5. Conclusions

TEM observations revealed the following defect microstructures and dehydroxylation mechanism of interstratified phyllosilicates recovered from a local podiform chromitite deposit in Taiwan.

(1) Phyllosilicates consist of interleaved chlorite–serpentine layers, dislocation, stacking fault, microcleavage and folding.

(2) Upon irradiation of electrons, the epitaxial magnesium hydroxide were formed after phyllosilicates and the microcracks were preferentially formed at interleaved areas, stacking faults and other defects.

(3) Microcracks extended along basal layers and coalesced to form larger cracks during dehydroxylation.

(4) Phyllosilicates decomposed finally into the periclase particles about several nm in size or probably other microcrystallites within the residual silica matrix.

Acknowledgement

We thank Dr D. R. Peacor for supplying his published papers about TEM observations of phyllosilicates. We also thank Mr R. C. Jeng for EPMA data.

References

1. A. F. MOODIE and C. E. WARBLE, *J. Crystal Growth* **74** (1986) 89.
2. G. M. ZHABROVA and V. A. GORDEEVA, *Kinetika i Kataliz, Akad. Nauk. SSSR, Sb. Statei*, (1960) 31.
3. S. J. GREGG and R. I. RAZOUK, *J. Chem. Soc.* S (1949) 36.
4. P. J. ANDERSON and R. F. HORLOCK, *Trans. Faraday Soc.* **58** (1962) 1993.
5. R. F. HORLOCK, P. L. MORGAN and P. J. ANDERSON, *ibid.* **59** (1963) 721.
6. R. C. TURNER, I. HOFFMAN and D. CHEN, *Can. J. Chem.* **41** (1963) 243.
7. R. S. GORDON and W. D. KINGERY, *J. Amer. Ceram. Soc.* **49** (1966) 654.
8. *Idem., ibid.* **50** (1967) 8.
9. G. W. BRINDLEY and M. NAKAHIRA, *ibid.* **40** (1957) 346.
10. J. L. EVANS and J. WHITE, *Trans. Br. Ceram. Soc.* **19** (1958) 289.
11. J. B. HOLT, I. B. CUTLER and M. E. WADSWORTH, *J. Amer. Ceram. Soc.* **45** (1962) 133.
12. J. F. GOODMAN, *Proc. R. Soc.* **A247** (1958) 346.
13. M. G. KIM, U. DAHMEN and A. W. SEARCY, *J. Amer. Ceram. Soc.* **70** (1987) 146.
14. J. L. BROWN and M. L. JACKSON, *Clays and Clay Minerals* **21** (1973) 1.
15. J. H. CHUTE and T. M. ARMITAGE, *Clay Minerals* **7** (1968) 455.
16. K. YADA, *Acta. Crystallogr.* **23** (1967) 704.
17. S. Y. LEE, M. L. JACKSON and J. L. BROWN, *Clays and Clay Minerals* **23** (1975) 125.
18. R. H. PAGE, *Contr. Miner. Petrol.* **75** (1980) 309.

19. D. R. VEBLEN and J. M. FERRY, *Amer. Miner.* **68** (1983) 1160.
20. J. OLIVES, M. AMOURIC, C. DE FOUQUET and A. BARONNET, *ibid.* **68** (1983) 754.
21. J. OLIVES and M. AMOURIC, *ibid.* **69** (1984) 869.
22. J. H. LEE, D. R. PEACOR, D. D. LEWIS and R. P. WINTSCH, *Contr. Miner. Petrol.* **88** (1984) 372.
23. J. H. LEE, J. H. AHN and D. R. PEACOR, *J. Sed. Petrology* **55** (1985) 532.
24. W. V. MARESCH, H. J. MASSONNE and M. CZANK, *Neues Jahrbuch Miner. Abh.* **152** (1985) 79.
25. M. AMOURIC, I. GIANETTO and D. PROUST, *Bull. Mineral.* **111** (1988) 29.
26. G. E. SPINNLER, D. G. SELF, S. IIJIMA and P. R. BUSECK, *Amer. Miner.* **69** (1984) 252.
27. M. AMOURIC, *Acta Crystallogr.* **B43** (1987) 57.
28. J. H. AHN, D. R. PEACOR and E. J. ESSENE, *Ultramicroscopy* **19** (1986) 375.
29. H. C. CHU, P. SHEN and R. C. JENG, *Proc. Geol. Soc. China* **31** (1988) 33.
30. M. CHO and J. J. FAWCETT, *Amer Miner.* **71** (1986) 68.
31. S. W. BAILEY and B. E. BROWN, *ibid.* **47** (1962) 819.
32. S. L. HWANG, P. SHEN, H. T. CHU and R. C. JENG, *Bull. Mineral* **111** (1988) 457.
33. I. D. R. MACKINNON and P. R. BUSECK, *Nature* **280** (1979) 219.
34. G. W. BRINDLEY and S. Z. ALI, *Acta Crystallogr.* **3** (1950) 25.
35. M. J. TSAI and P. SHEN, *Mater. Sci. Eng.* **83** (1986) 135.
36. G. N. SUBBANNA and T. R. N. KUTTY, *Mater. Chem. Phys.* **13** (1985) 97.
37. D. BERUTO, P. F. ROSSI and A. W. SEARCY, *J. Phys. Chem.* **89** (1985) 1695.

Received 21 February
and accepted 30 August 1989